

Structural and optical properties of MBE-grown asymmetric cubic GaN/Al_xGa_{1-x}N double quantum wells

T. Wecker^{*1}, F. Hörich², M. Feneberg², R. Goldhahn², D. Reuter¹, and D. J. As¹

¹ Department of Physics, University of Paderborn, Warburger Strasse 100, 33098 Paderborn, Germany

² Institute of Experimental Physics, Otto von Guericke University, Universitätsplatz 2, 39106 Magdeburg, Germany

Received 18 September 2014, revised 6 November 2014, accepted 7 November 2014

Published online 22 December 2014

Keywords III-nitride semiconductors, charge carriers, molecular beam epitaxy, optical properties, quantum wells, tunneling

* Corresponding author: e-mail wtobias@mail.uni-paderborn.des, Phone: +49 5251 605831, Fax: +49 5251 605843

The non-resonant carrier transfer in asymmetric double quantum wells is studied. Asymmetric cubic GaN/Al_xGa_{1-x}N double quantum wells with Al content of $x = 0.26 \pm 0.03$ were grown on 3C-SiC (001) substrate by radio-frequency plasma-assisted molecular beam epitaxy. The barrier thickness d between a wide quantum well having 2.5 nm thickness and a narrow quantum well with width of 0.7 nm was varied from 1 to 15 nm. Furthermore, high resolution X-ray diffraction reciprocal space maps around the (113) direction provided the Al content and revealed a partially strain in the Al_xGa_{1-x}N barriers and QWs. The coupling between the QWs was studied by interband photoluminescence spectroscopy at low temper-

atures. Four clearly distinguishable emission bands at 3.27 eV, 3.37 eV, 3.60 eV, and 3.74 eV are observed and could be assigned to the different layers. With decreasing barrier thickness d the photoluminescence intensity from the narrow QW is strongly reduced, indicating wave function redistribution from the narrow QW to the wide QW. The emission energies for the QWs are in good agreement with theoretical calculations using a Schrödinger–Poisson solver based on an effective mass model (nextnano³). The PL intensity ratio of the narrow QW to the wide QW for varied barrier thicknesses was calculated by exploiting rate equations, revealing a good agreement between theory and experiment.

© 2014 WILEY-VCH Verlag GmbH & Co. KGaA, Weinheim

1 Introduction Recently group III-nitrides and their compounds have been exploited for THz devices, fast modulators and fast photo detectors [1]. Due to the large band offset of GaN/AlN heterostructures, these materials are suitable for devices based on intersubband transitions in the 1.55 μm spectral region (optical C-band) [2]. Using Al_xGa_{1-x}N as compound material enables another degree of freedom for designing the needed energy levels in the QWs for such complex devices. For modern optoelectronic devices based on intersubband transitions like Quantum Cascade Lasers (QCLs) [2] a suitable intersubband transition (ISBT) carrier transfer between coupled QWs through thin barriers is of paramount importance.

Hexagonal group III nitrides suffer from large internal polarization fields along the c-axis resulting in a bending of the bands and in the internal quantum confined Stark-effect. Hence the design of modern devices for intraband transitions in this system is rather complicated [3]. Furthermore, the electron and hole wave functions are spatially separated, thus the efficiency

of devices based on interband emission is reduced. As a result, great effort is made reducing this effect by growing semi-polar group III nitrides in the hexagonal phase [4]. Another approach is growing cubic group III nitrides in the (001) direction on 3C-SiC. This avoids the unfavorable effects discussed above completely along the growth axis. Recent advantages in the growth of multi quantum well structures of cubic group III-nitrides lead to the observation of ISBT in the near-infrared and THz spectral range [1, 5, 6].

In this work, we study the non-resonant carrier transfer in cubic GaN/Al_xGa_{1-x}N asymmetric double quantum wells (ADQWs) by measuring the intensity ratio of the photoluminescence (PL) emission from the narrow and the wide QW as a function of the thickness of the barrier. Model calculations of the transition energies were performed with nextnano[3, 7]. A rate equation model was used for the carrier transfer between the two QWs. Both the calculated transition energies as well as the evaluated tunneling rates are in reasonable agreement with the experimental data.

2 Experimental

2.1 Sample description Asymmetric cubic GaN/Al_xGa_{1-x}N double quantum wells with an Al content of $x = 0.26 \pm 0.03$ were grown on a 10 μm 3C-SiC (001) layer deposited on a 1 mm thick Si substrate. For the growth a Riber-32 radio-frequency plasma-assisted molecular beam epitaxy (PAMBE) system was used adapted with standard effusion cells for Ga and Al evaporation. Atomic nitrogen is provided by an Oxford plasma source and the growth process is *in situ* controlled by Reflection High Energy Electron Diffraction (RHEED). The growth of c-GaN and c-Al_xGa_{1-x}N was realized at a substrate temperature of $T_S = 720^\circ\text{C}$ under one monolayer of Ga excess on the surface. More details concerning the growth of cubic GaN on 3C-SiC can be found in Ref. [8]. AFM measurements revealed an rms surface roughness reaching from 1.9 nm to 2.6 nm for $5 \times 5 \mu\text{m}^2$ areas.

Directly on the 3C-SiC substrate a 130 nm thick c-GaN buffer layer was grown. The buffer layer is followed by the asymmetric double quantum well structure. The barrier thickness d between a wide quantum well (QW_W) having 2.5 nm thickness and a narrow quantum well (QW_N) of width of 0.7 nm was varied between 1 and 15 nm (see Table 1). The ADQW structure is situated between two 50 nm thick cubic Al_{0.26}Ga_{0.74}N layers. The sample structure is shown in Fig. 1.

Table 1 List of samples with barrier thickness d , the Al content x and the degree of relaxation R of the Al_xGa_{1-x}N barriers.

sample	barrier thickness d [nm]	Al content x	degree of relaxation R
A1	1	0.26 ± 0.03	0.40 ± 0.05
A2	3	0.27 ± 0.03	0.38 ± 0.05
A3	5	0.26 ± 0.03	0.41 ± 0.05
A4	10	0.26 ± 0.03	0.38 ± 0.05
A5	15	0.25 ± 0.03	0.39 ± 0.05

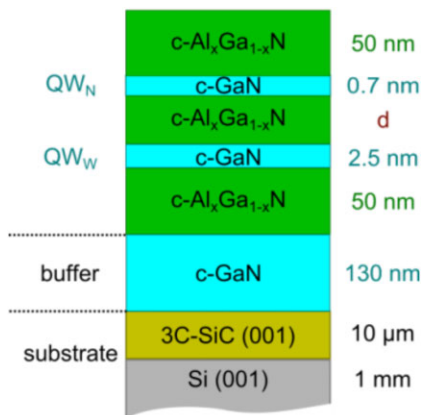


Figure 1 Sample structure of the cubic GaN/Al_xGa_{1-x}N ADQWs. The barrier thickness d was varied from 1 nm to 15 nm and the Al content is $x = 0.26 \pm 0.03$.

2.2 Structural properties Structural properties were characterized by high-resolution X-ray diffraction (HRXRD) reciprocal space map (RSM) measurements. The defect density of the order of $D = 2 \times 10^{10} \text{ cm}^{-2}$ was determined by rocking curve full width half maxima around the (002) reflection. From the RSM around the (113) reflection of the ADQW sample with $d = 15 \text{ nm}$ an Al content of $x = 0.25 \pm 0.03$ could be determined (see Fig. 2). Besides small variations the Al content of the Al_xGa_{1-x}N barriers of all samples is $x = 0.26 \pm 0.03$ (see Table 1). From the RSM measurements also the degree of relaxation R of the layers is provided. All Al_{0.26}Ga_{0.74}N layers are partly tensilely strained ($R = 40\%$) to the GaN buffer layer (see Table 1), thus an equilibrium lattice parameter is formed in the ADQW structure leading to partly compressively strained QWs.

2.3 Nextnano³ simulations Band structure calculations are needed for a deeper insight into intraband transitions and carrier transfer phenomena. A Schrödinger–Poisson solver (nextnano³ [7]) was used to calculate the energy levels of the ADQW as well as the interband transitions. Band structure calculations with nextnano³ (nn³) are based on an effective mass model. The ratio of the conduction band offset to the valence band offset (CBO: VBO) used is 74:26 [9] and the bowing parameter for Al_xGa_{1-x}N is $b = -0.85 \text{ eV}$ [10]. The parameters used for the nextnano³ simulations are summarized in Table 2. For Al_xGa_{1-x}N all values are linearly interpolated except for the band gaps. In all calculations, a background n-type doping of around $5 \times 10^{17} \text{ cm}^{-3}$ in Al_xGa_{1-x}N and of around $1 \times 10^{17} \text{ cm}^{-3}$ in GaN is assumed [11].

Furthermore, the partially compressively strained QWs and the tensilely strained Al_xGa_{1-x}N barriers are taken into account in the simulations.

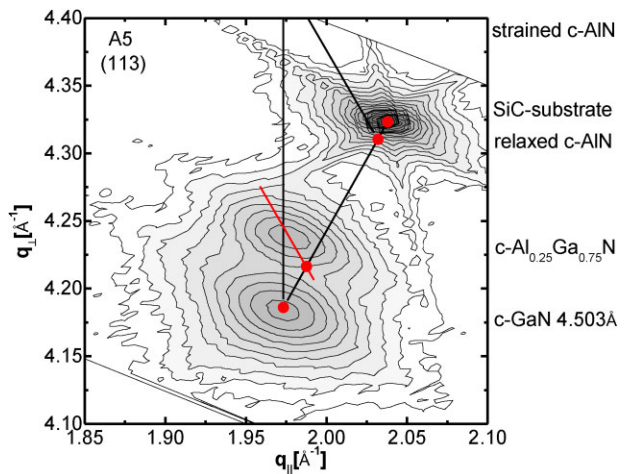


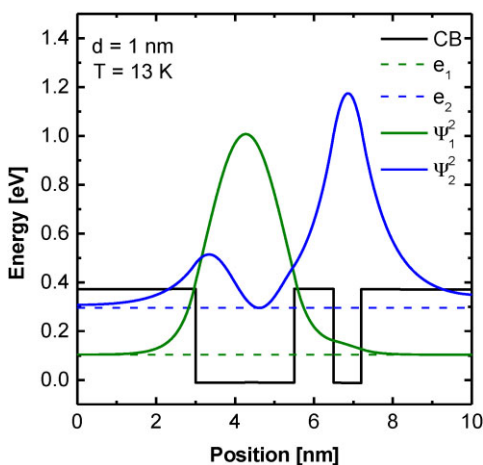
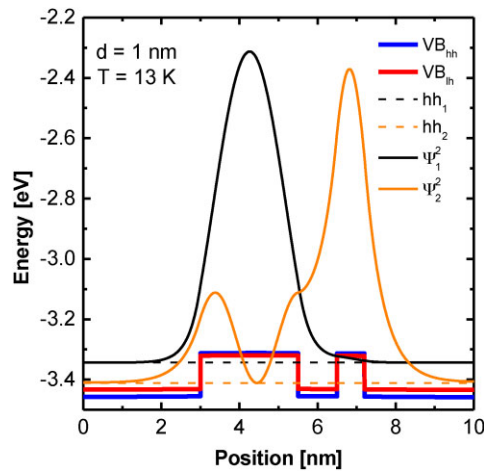
Figure 2 Reciprocal space map of the (113) reflex of the cubic GaN/Al_xGa_{1-x}N ADQW A5 with $d = 15 \text{ nm}$. An Al content of $x = 0.25 \pm 0.03$ is determined and a partial strain of the barriers is visible.

Table 2 Parameters used for nextnano³ simulations.

parameter	c-GaN	c-AlN
$E_{\text{gap, 0K}}$ [eV]	3.293 [13]	5.997 [14]
$E_{\text{gap, 300K}}$ [eV]	3.23 [13]	5.93 [16]
a [Å]	4.503 [15]	4.373 [17]
m_e^*/m_0	0.19 [18]	0.3 [18]
m_{hh}^*/m_0	0.83 [18]	1.32 [18]
m_{lh}^*/m_0	0.28 [18]	0.44 [18]
m_{so}^*/m_0	0.34 [18]	0.55 [18]
a_c [eV]	-2.77 [19]	-6.8 [19]
a_v [eV]	2.0 [21]	2.3 [21]
b_{uniax} [eV]	-1.7 [21]	-1.5 [21]
c_{11} [GPa]	293 [20]	304 [20]
c_{12} [GPa]	159 [20]	160 [20]
c_{44} [GPa]	155 [20]	193 [20]
Δ_{so} [meV]	15 [13]	19 [26]

The simulated transition energies at 13 K for the narrow and the wide well are $E_{\text{sim}}^{\text{N}} = (3.70 \pm 0.09)$ eV and $E_{\text{sim}}^{\text{W}} = (3.45 \pm 0.04)$ eV. In the nn³ calculations, no excitonic effects are considered. They are calculated independently analog to [12] and are taken into account afterwards. The calculated excitonic binding energies in the QW_N are $E_{\text{ex}}^{\text{N}} = (57 \pm 9)$ meV and for the QW_W $E_{\text{ex}}^{\text{W}} = (46 \pm 7)$ meV. In the growth of the quantum wells, the well thickness frequently differs by ± 1 monolayer (one monolayer (1ML) of cubic GaN is 0.225 nm). The nn³ simulations predict for a variation of the well width of ± 1 ML an energy shift of ± 15 meV for the QW_W and ± 40 meV for the QW_N, respectively.

In Fig. 3 and Fig. 4 the conduction band edge and the valence band edges for electrons (e), heavy holes (hh) and light holes (lh) together with the probability distribution $|\Psi|^2$ for e and hh are plotted vs. position for the ADQW structure with a barrier thickness of 1 nm. For clarity, the band

**Figure 3** Simulation results of the conduction band of the cubic GaN/Al_xGa_{1-x}N ADQW with $x=0.26$ and a barrier thickness $d=1$ nm at 13 K.**Figure 4** Simulation results of the heavy hole (hh, blue) and light hole (lh, red) valence bands of the cubic GaN/Al_xGa_{1-x}N ADQW with $x=0.26$ and a barrier thickness $d=1$ nm at 13 K. The probability distribution $|\Psi|^2$ is plotted for the hh only.

diagrams for the conduction band and the valence band have been drawn separately. In this presentation, the energy zero is defined as conduction band edge of cubic GaN. Electrons in the wide QWs are confined above the conduction band by about 0.1 eV and electrons in the narrow QWs by about 0.3 eV as indicated in Fig. 3 by the dashed lines e_1 and e_2 , respectively. As indicated by the probability distribution $|\Psi_1|^2$ of the electrons in the ground state e_1 of the wide QW (green curve) and $|\Psi_2|^2$ of the electrons in the ground state e_2 of the narrow QW (blue curve) the penetration depths of the corresponding wave functions are much larger than the barrier thickness. Therefore, a clear coupling of the two QWs is proposed and wave function redistribution which can be described by non-resonant tunneling of the electrons is expected.

In Fig. 4 equivalent calculations of the band diagram for the heavy holes in the cubic GaN/Al_xGa_{1-x}N ADQW with a 1 nm thick barrier thickness are depicted (blue curve). The quantization energies for the wide and the narrow QW are about 56 meV and 100 meV measured from the hh valence band of GaN, respectively. Similar to the situation for the electrons the wave function for the heavy holes in the states hh_1 and hh_2 penetrate into the neighboring QW suggesting significant coupling of the two QW states.

Due to the residual strain in the QW structure the band gaps for heavy and light holes are slightly different. The characteristics of the valence band edge diagram for hh and lh are also shown in Fig. 4 (blue curve for hh valence band and red curve lh valence band). However, since the quantization energy of the light holes will be larger due to their lower effective masses we expect that for PL measurements no e–lh transitions will be observable at low temperature.

Additional calculations for the other GaN/Al_xGa_{1-x}N ADQW structures with wider barrier thicknesses showed

that coupling is relevant for barrier thicknesses below 4 nm only. For thick barriers of $d > 10$ nm³ simulations indicate that no significant coupling will occur.

For optical recombination processes as observed in PL, the carrier redistribution of both electrons and holes is relevant to explain the observed changes in PL emission intensity.

2.4 Optical properties Figure 5 depicts the low temperature interband photoluminescence measurements at 13 K for sample A5 with $d = 15$ nm in a semi-logarithmic plot. For excitation, a Nd:YAG cw laser with two frequency doubling steps emitting at 4.66 eV (266 nm) was used. Four clearly distinguishable emission bands at 3.27 eV, 3.37 eV, 3.60 eV and 3.74 eV are observed. Using four Gaussian fit functions, the emission bands were determined and they could be assigned to the c-GaN buffer [13], the wide QW_W, the narrow QW_N, and the cubic Al_{0.26}Ga_{0.74}N [10], respectively. The transition energies of both QWs are consistent with our calculations by nn³.

In Figure 6, the low temperature PL spectra of GaN/Al_{0.26}Ga_{0.74}N ADQWs with different barrier thicknesses d are shown. For better comparison, the PL spectra have been normalized to the emission of the Al_{0.26}Ga_{0.74}N at 3.74 eV and are plotted in a semi-logarithmic scale. It can be seen clearly that under identical excitation conditions the intensity of the narrow QW I_N becomes weaker whereas the intensity of the wider QW I_W increases with decreasing barrier thickness. This is a clear indication that wave function redistribution is a relevant effect. The energy shift of the emission of the wide QW for the sample A1 with the lowest barrier thickness $d = 1$ nm (pink curve) may be due to a slightly thicker QW width. The sample A4 with $d = 10$ nm (blue curve) shows a strong broadening of the emission band

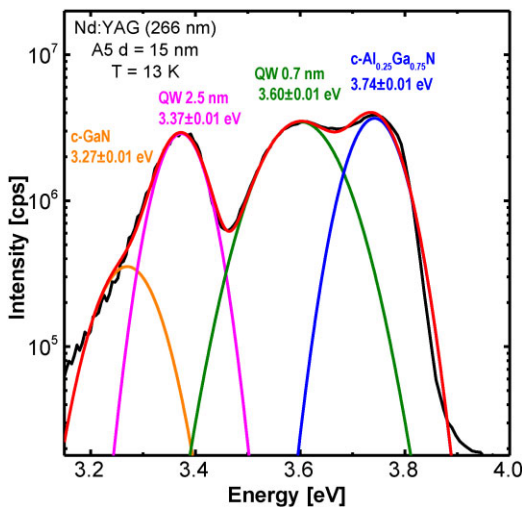


Figure 5 Semi-logarithmic plot of the low temperature PL spectrum of the cubic GaN/Al_{0.26}Ga_{0.74}N ADQW A5 with $d = 15$ nm. For excitation a Nd:YAG cw laser with a wavelength of 266 nm was used.

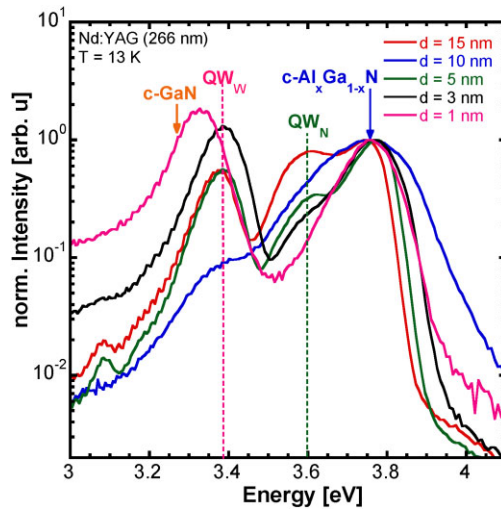


Figure 6 Low-temperature PL spectra of the cubic GaN/Al_{0.26}Ga_{0.74}N ADQWs normalized to the emission of Al_{0.26}Ga_{0.74}N at 3.74 eV. The barrier thickness d varies between 15 nm and 1 nm.

related to the AlGaN emission and the intensity of the wide QW emission is decreased compared to the other samples. The AFM, HRXRD and RHEED data of this sample are consistent with the data of the other samples. But the PL measurements show a fluctuation of the intensities of the emission bands for different positions at this sample piece. This effect is still under investigation.

In the following, the intensities will be described by a formalism of tunneling rates $T(d)$ for electrons and holes for barrier thicknesses d [22]

$$T(d) = \frac{T_0 4kE(V-E)}{4kE(V-E) + ((k-1)E+V)^2 \sinh^2\left(\frac{d}{\lambda}\right)} \quad (1)$$

where $T_0 = \frac{h}{4m_{\text{well}}L_z^2}$, $k = \frac{m_{\text{barrier}}}{m_{\text{well}}}$ and $\lambda = \frac{\hbar}{\sqrt{2m_{\text{barrier}}(V-E)}}$; T_0 is the classical period of the electron or hole motion in a well of thickness L_z , k is the effective mass ratio of the carriers, and λ is the penetration depth of the wave functions into the barriers, respectively. The energy levels of the carriers E are provided by nn³ simulations and V is the barrier height.

We analyze the experimental results by considering the following processes. Light of the excitation source is absorbed creating electron hole pairs in the two QWs and in the surrounding barrier material, the carriers in the barriers diffuse into the QW_W and QW_N. These processes are described by generation rates G_W and G_N . A fraction of the generated carriers in the narrow well is tunneling through the barrier into the wide well with the tunneling rate $T(d)$, and the rest recombines radiatively with lifetime τ_N . The ground state in the wide QW is about 200 meV lower than in the narrow well. This leads to the following rate

equation of carrier densities in the narrow (n_N) and the wide (n_W) well:

$$\frac{dn_N}{dt} = G_N - \frac{n_N}{\tau_N} - T(d)n_N, \quad (2)$$

$$\frac{dn_W}{dt} = G_W - \frac{n_W}{\tau_W} + T(d)n_W, \quad (3)$$

and for holes accordingly [22]. Using the steady state solutions of the above equations, the ratio of the intensities I_N to I_W is given by

$$\frac{I_N}{I_W} = \frac{\frac{\tau_W}{\tau_N}}{\left(1 + \frac{G_W}{G_N}\right)\tau_W T(d) + \frac{G_W \tau_W}{G_N \tau_N}}, \quad (4)$$

where τ_W and τ_N are the radiative lifetimes in the two quantum wells [22]. Recent results of time resolved PL measurements on decoupled samples estimate that the life times in both QWs are on the order of $\tau \approx 180$ ps [24]. For the ratio of the generation rates, the best match with the experimental data for the uncoupled QW with $d = 15$ nm is found to be $G_W/G_N = 0.55$. These values have been applied to equation (4).

For $\text{Al}_{0.26}\text{Ga}_{0.74}\text{N}$ the ratio of the effective masses of electrons and heavy holes is only different by a factor of 4.5 and the barrier potential V for electrons is about 4 times higher than that for holes. Therefore, the carrier-tunneling rate is expected to be in the same order of magnitude for both types of carriers. For that reason, we calculated the tunneling rate for both electrons and holes. In Table 3 values for the penetration depth λ , T_0 , and $T(d)$ for different barrier thicknesses are given for electrons and heavy holes, respectively. Since in our cubic GaN QWs, the electron and hole tunneling rates are comparable, photo-induced space charge built-up effects may be negligible in contrast to the case of asymmetric InGaAs/InP QWs [25].

Furthermore, for the low temperature, PL measurements the defects are not ionized, thus as an approximation the non-radiative recombination is neglected in this simple model. A quantitative investigation for the decay times of the

Table 3 Calculated values of the penetration depth λ , T_0 , and the tunneling rate $T(d)$ for electrons (e) and heavy holes (hh), respectively.

	e	hh
λ [nm]	0.7976	0.8297
T_0 [s^{-1}]	2.1×10^{15}	4.8×10^{14}
$T(15 \text{ nm})$ [s^{-1}]	3.4×10^{-1}	3.6×10^{-1}
$T(10 \text{ nm})$ [s^{-1}]	9.4×10^4	6.2×10^4
$T(5 \text{ nm})$ [s^{-1}]	2.6×10^{10}	1.1×10^{10}
$T(3 \text{ nm})$ [s^{-1}]	3.9×10^{12}	1.3×10^{12}
$T(1 \text{ nm})$ [s^{-1}]	5.3×10^{14}	1.4×10^{14}

different layers exploiting time dependent PL measurements is still in progress.

Figure 7 depicts the intensity ratio of the emission from the narrow QW to that from the wide QW as a function of barrier thickness d . A reduction in the intensity ratio is observed only for barriers thinner than 4 nm. In structures with broader barriers, the two QWs are effectively decoupled and a constant I_N to I_W ratio is found. For radiative recombination processes presence of both electrons and holes is necessary. Therefore, the carrier type with lower tunneling rate is expected to limit the finally observed equilibrium intensity ratio in the steady state PL measurements.

Using Eq. (4), the intensity ratio is calculated for the carrier transfer processes limited by electron tunneling (blue curve) and hole tunneling (red curve). As expected, the limiting hole tunneling process fits better to the experimental data than the electron tunneling process. The overall behavior is well explained, however for low barrier thicknesses a deviation from the calculations is seen, indicating a reduced tunneling rate (higher I_N to I_W ratio) for thin barriers.

The difference between model and experiment can be explained partly by an uncertainty of 5% for the band offset at the GaN/AlGaN interfaces and the inaccuracy of an Al content in the barrier of $x = 0.26 \pm 0.03$. Thickness fluctuations in the QWs, which may be responsible for the observed relative broad PL emissions have also to be considered. Finally, scattering of carriers by defects in the barriers may increase the transfer time and increase the I_N to I_W ratio. Taking all these effects into account, the experimental data are in good agreement with the proposed simple model.

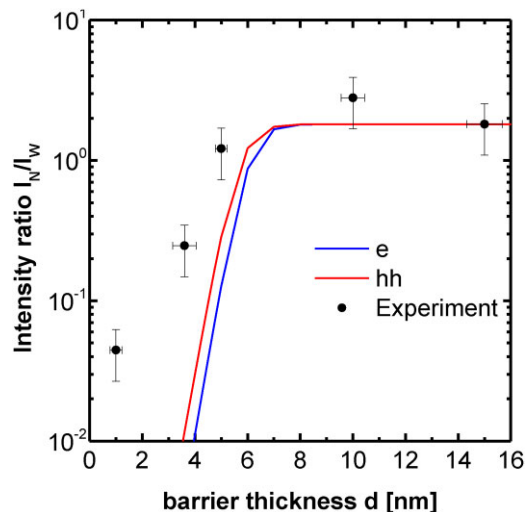


Figure 7 Intensity ratio I_N/I_W as a function of barrier thickness d . The full dots represent measured intensity ratios and the continuous lines show calculated intensity ratios by Eq. (4) for electrons (e) (blue line) and heavy holes (hh) (red line).

3 Conclusion Asymmetric cubic GaN/Al_{0.26}Ga_{0.74}N double quantum wells with systematic variation of the barrier thickness d were grown by plasma assisted molecular beam epitaxy. HRXRD measurements provide the Al content of $x = 0.26 \pm 0.03$. A partial strain of the Al_{0.26}Ga_{0.74}N barriers is observed in the RSMs around the (113) reflection, leading to an equilibrium lattice parameter with tensilely strained Al_xGa_{1-x}N barriers and compressively strained QWs. PL measurements of an uncoupled QW structure revealed four clearly resolvable emission bands, which could be attributed to originate in the different layers. ADQW structures with barrier thickness below 4 nm exhibit a clear change in the PL intensity ratio, indicating considerable redistribution of wave functions. The carrier transfer is described by a simple tunneling model considering both electrons and holes. Using the energy levels calculated with nextnano³ and applying rate equations [22] for the recombination of electrons and heavy holes in the two QWs, the barrier thickness dependence of the ratio of the emission intensities I_N to I_W is reproduced. However, for very narrow barriers, the comparison between theory and experimental data reveal a deviation to our simple model. Nevertheless, the theoretical and experimental results are in good agreement.

Acknowledgements This work has been financially supported by the Deutsche Forschungsgemeinschaft (DFG) via TRR142 and by the Center for Optoelectronics and Photonics Paderborn (CeOPP).

References

- [1] H. Machhadani, M. Tchernycheva, L. Rigutti, S. Saki, R. Colombelli, C. Mietze, D. J. As, and F. H. Julien, *Phys. Rev. B* **83**, 075313 (2011).
- [2] C. Gmachl and H. M. Ng, *Electron. Lett.* **39**, 567 (2003).
- [3] M. Beeler, C. Bougerol, E. Bellet-Amalric, and E. Monroy, *Phys. Status Solidi A* **211**(4), 761–764 (2014).
- [4] F. Scholz, *Semicond. Sci. Technol.* **27**, 024002 (2012).
- [5] D. J. As and C. Mietze, *Phys. Status Solidi A* **210**, 474 (2013).
- [6] C. Mietze, M. Bürger, S. Sakr, M. Tchernycheva, F. H. Julien, and D. J. As, *Phys. Status Solidi A* **210**, 455 (2013).
- [7] S. Birner, S. Hackenbuchner, M. Sabathil, G. Zandler, J. A. Majewski, T. Andlauer, T. Zibold, R. Morschl, A. Trellakis, and P. Vogl, *Acta Phys. Polon. A* **110**, 111 (2006).
- [8] J. Schörmann, S. Potthast, D. J. As, and K. Lischka, *Appl. Phys. Lett.* **90**, 041918 (2007).
- [9] C. Mietze, M. Landmann, E. Rauls, H. Machhadani, S. Sakr, M. Tchernycheva, F. H. Julien, W. G. Schmidt, K. Lischka, and D. J. As, *Phys. Rev. B* **83**, 195301 (2011).
- [10] M. Landmann, E. Rauls, W. G. Schmidt, M. Röppischer, C. Cobet, N. Esser, T. Schupp, D. J. As, M. Feneberg, and R. Goldhahn, *Phys. Rev. B* **87**, 195210 (2013).
- [11] D. Bouguenna, A. Boudghene Stambouli, N. Mekakia Maaza, A. Zado, and D. J. As, *Superlattices Microstruct.* **62**, 260 (2013).
- [12] H. Mathieu, P. Lefebvre, and P. Christol, *Phys. Rev. B* **46**, 4093 (1992).
- [13] M. Feneberg, M. Röppischer, C. Cobet, N. Esser, J. Schörmann, T. Schupp, D. J. As, F. Hörich, J. Bläsing, A. Krost, and R. Goldhahn, *Phys. Rev. B* **85**, 155207 (2012).
- [14] In h-AlN the difference in the energy gap from 0 K to 300 K is about 67 meV [26, 23]. A similar value for c-AlN is assumed leading to $E_{\text{gap, 0K}} = E_{\text{gap, 300K}} + 67 \text{ meV}$.
- [15] K. Kim, W. R. L. Lambrecht, and B. Segall, *Phys. Rev. B* **53**, 16310 (1996).
- [16] M. Röppischer, R. Goldhahn, G. Rossbach, P. Schley, C. Cobet, N. Esser, T. Schupp, K. Lischka, and D. J. As, *J. Appl. Phys.* **106**, 076104 (2009).
- [17] T. Schupp, K. Lischka, and D. J. As, *J. Cryst. Growth* **312**, 1500 (2010).
- [18] L. C. de Carvalho, A. Schleife, and F. Bechstedt, *Phys. Rev. B* **84**, 195105 (2011).
- [19] S. H. Park and S. L. Chuang, *J. Appl. Phys.* **87**, 353 (2000).
- [20] A. F. Wright, *J. Appl. Phys.* **82**, 2833 (1997).
- [21] C. G. V. de Walle and J. Neugebauer, *Appl. Phys. Lett.* **70**, 2577 (1997).
- [22] T. Tada, A. Yamaguchi, T. Ninomiya, H. Uchiki, T. Kobayashi, and T. Yao, *J. Appl. Phys.* **63**, 5491 (1988).
- [23] M. Feneberg, M. F. Romero, M. Röppischer, C. Cobet, N. Esser, B. Neuschl, K. Thonke, M. Bickermann, and R. Goldhahn, *Phys. Rev. B* **87**, 235209 (2013).
- [24] T. Wecker, privat communication.
- [25] R. Sauer, K. Thonke, and W. T. Tsang, *Phys. Rev. Lett.* **61**, 609 (1988).
- [26] I. Vurgaftman and J. R. Meyer, *J. Appl. Phys.* **94**, 3675 (2003).